Supplementary Information

Dendrite Growth and Inhibition in All-Solid-State Lithium Metal Battery: In-situ Optical Observation

*Haowen Liu, Weining Jiang, Wenjie Chen, Qiyuan Lin, Shuaiyang Ren, Yipeng Su, Ruoyu Tong, Yuegang Zhang**

State Key Laboratory of Low-Dimensional Quantum Physics, Department of Physics, Tsinghua University, Beijing, 100084, China

Frontier Science Center for Quantum Information, Beijing, 100084, China

E-mail: yuegang.zhang@tsinghua.edu.cn

1. Experimental Section

1.1 Synthesis of LPSC-PTFE and LPSC-LiF composite electrolytes

The LPSC-PTFE composite electrolyte was prepared by grinding 100 mg LPSC (Kejing) and 10 mg PTFE (Kejing) in a mortar for 30 minutes to obtain a flexible and homogeneous membrane. Preparation of LPSC-LiF composite electrolytes, firstly, considering that the density of LPSC is 1.64 g cm^{-3} and the density of LiF is 2.64 g cm^{-3}, LPSC and LiF (Aladdin) with corresponding mass ratios are weighed according to different nominal volume ratios and pre-ground in a mortar for 30 minutes. Then, the obtained powder is ground by a ball mill at a speed of 200 rpm for 1 h. The LPSC-LiF composite electrolytes were labeled as PF81, PF61 and PF41 according to the nominal volume ratio of LPSC to LiF, and "LPSC-LiF" in this article refers to the PF61 if not specified otherwise. All synthesis experiments were conducted in an argon-filled glove box with water and oxygen concentrations less than 0.5 ppm.

1.2 Assembly of All-solid-state cells

1.2.1 Assembly of Li|LPSC|LPSC-PTFE|LPSC|Cu cells for in situ optical observation

Firstly, the prepared LPSC-PTFE composite electrolyte was pressed into a 10 mm cylindrical quartz mold between the two Stainless steel rods at 300 MPa for 10 min. Then, 30 mg and 200 mg LPSC electrolyte were pressed on the upper and lower sides of the LPSC-PTFE layer at 300 MPa for 10 min, respectively. Then, a lithium foil with a diameter of 10 mm and a thickness of 400 μm is attached to the 200 mg LPSC electrolyte layer, and a 20 μm Cu foil with a diameter of 10 mm is attached to the 30 mg LPSC electrolyte layer. Note that a tape with a diameter of 9 mm is placed in the center of the Cu foil (Figure S2b). Finally, the assembled Li|LPSC|LPSC-PTFE|LPSC|Cu was sealed into the stainless-steel mold with a pressure of 30 MPa.

1.2.2 Assembly of Li|LPSC|Cu and Li|LPSC-LiF composite electrolytes |Cu cells.

Firstly, LPSC electrolyte (100 mg) /PF81(106.8 mg)/ /PF61(108.7 mg)/ /PF41(112.2 mg) was pressed into a 10 mm cylindrical polyether ether keptone (PEEK) mold between the two Stainless steel rods at 300 MPa for 10 min. Subsequently, the thick lithium foil with a thickness of 400 μm is pressed with a pressure of 1.5 GPa into a thin lithium foil with a thickness of about 120 μm. Then, a thin lithium foil with a diameter of 10 mm was rushed out with a punch, and attached to one side of the LPSC electrolyte layer. A 20 μm Cu foil with a diameter of 10 mm is attached to the other side of the LPSC electrolyte layer. Finally, the assembled Li|LPSC|Cu was sealed into the stainless-steel mold with a pressure of 30 MPa. It

should be noted that the thickness of lithium foil used is 400 μm when the current density of plating is 1 mA cm^{-2}.

1.2.3 Assembly of Li|LPSC|Li and Li|LPSC-LiF|Li cells.

The assembly of Li|LPSC|Li and Li|LPSC-LiF|Li cells is similar to the assembly of Li|LPSC|Cu and Li|LPSC-LiF|Cu cells, except that the copper foil is replaced by lithium foil.

1.2.4 Assembly of Li|LPSC|LPSC-PTFE|LPSC|Cu and Li|LPSC|LPSC-PTFE|LPSC-LiF|Cu cells for verify the dendrite blocking ability of LPSC-LiF electrolyte.

The assembly of Li|LPSC|LPSC-PTFE|LPSC|Cu cell was the same as above, but both layers of LPSC electrolyte are 30 mg, and the assembly of Li|LPSC|LPSC-PTFE|LPSC-LiF|Cu cells was only to replace the LPSC electrolyte layer near the Cu side with about 33 mg LPSC-LiF electrolyte.

1.2.5 Preparation of $LiCoO_2$ cathode and Assembly of Li |LPSC| $LiCoO_2$ and Li|LPSC-LiF| $LiCoO_2$ cells.

The preparation of $LiCoO_2$ cathode: LiInCl electrolyte (Kejing), Super P and $LiCoO_2$ powders were mixed uniformly by hand milling for 30 min at the mass ratio of m electrolyte: m $LiCoO_2$: m C = 70:30:6, to yield a black mixture.

Assembly of Li|LPSC|$LiCoO_2$ and Li|LPSC-LiF|$LiCoO_2$ cells: LPSC electrolyte (100 mg) /PF61(108.7 mg) was pressed into a 10 mm cylindrical PEEK mold between the two Stainless steel rods at 300 MPa for 10 min. Then, 10 mg cathode powder was pressed on one side of the electrolyte layer at 150 MPa for 10 min. Then, a thin lithium foil with a diameter of 10 mm was attached to the other side of the electrolyte layer. Finally, the assembled Li|LPSC|$LiCoO_2$ or Li|LPSC-LiF|$LiCoO_2$ was sealed into the stainless-steel mold with a pressure of 30 MPa.

2. Electrochemical Measurement

Electrochemical impedance spectroscopy (EIS) characterization of Li|SSEs|Li cells were assembled for evaluating the electrochemical impedance. It was conducted within the range of 1 MHz to 1 Hz with amplitude of 10 mV， and EIS profiles was obtained on an Autolab PGSTAT204. SS|SSEs|SS symmetric cells were fabricated for evaluating the electronic conductivity of SSEs, and it was conducted with a voltage of 0.5 V on a Keysight B2912A.

Li|SSEs|Cu asymmetric cells were assembled to verify the ability of different electrolytes to inhibit dendrites. The cells were discharged at a current density of 0.02, 0.05, 0.3 or 0.5 mA cm^{-2}. Li|SSEs|Li symmetric cells were fabricated for evaluating the ability to inhibit dendrites and long-cycle performances of SSEs, which were performed at current densities of 0.3 mA cm^{-2} and 0.5 mA cm^{-2}. Li|LPSC|$LiCoO_2$ and Li|LPSC-LiF|$LiCoO_2$ cells were fabricated for evaluating the ability to inhibit dendrites of SSEs during long cycle, which were performed at a test rate of 0.1 C. All the cells were evaluated on a Land CT2001 automatic battery tester at room temperature.

3. Materials Characterizations

In situ optical characterization was performed with the asanas microscope Stereozoom S9D. Scanning electron microscopy (SEM) and energy-dispersive spectrometry (EDS) experiments were carried out with a field emission scanning electron microscope (Sirion 200). X-ray diffraction (XRD) was carried out with a scanning rate of 4°/min from 20° to 80° to characterize the structure of SSEs. Cu *K*α radiation with an average wavelength 1.54059 Å was used as the radiation source.

4. Theoretical calculations

Density functional calculations were performed using the Vienna Ab Initio Simulation Package (VASP). [1] Potentials were generated via the projector augmented wave (PAW) [2] pseudopotential within Perdew−Burke−Ernzerhof (PBE) [3] exchange−correlation functional. All calculations were performed with a cutoff energy of 600 eV. The convergence criteria for electronic and ionic relaxation were set to 10^{-6} eV per unit cell and 0.05 eV per Å, respectively. A Monkhorst-Pack k-points mesh with a k-spacing of 0.3 $Å^{-1}$ was used for k-space sampling.

Primitive crystal structures were obtained from the Materials Project and used for cell relaxation before establishing supercells and stack interface structures. [4] To calculate interface energy (γ_{AB}) and interfacial adhesion energy (W_{AB}), the equations below were used:

$$\gamma_{AB} = \frac{E_{AB} - n_A E_A - n_B E_B}{2S}$$

$$W_{AB} = \gamma_A + \gamma_B - \gamma_{AB}$$

E_{AB} represents the calculated energy of this configuration. $\gamma_A(\gamma_B)$ is the surface energy of substance A(B), while $E_A(E_B)$ is the bulk energy of substance A(B), $n_A(n_B)$ is the number of A(B) atoms, respectively. [5]

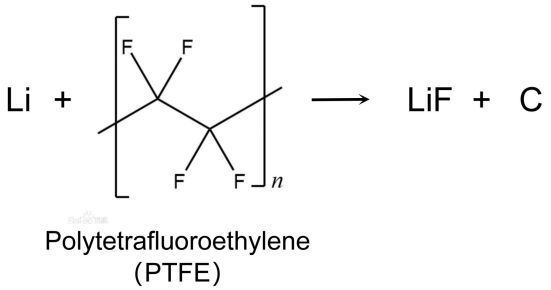

Figure S1. Reaction formula of Li and PTFE

However, PTFE is known to readily accept electrons and convert to carbine-type carbon through defluorination by the chemical reaction with alkali metals, and the carbine-type carbon is easily transformed to electrically conducting sp2 carbon. [6]

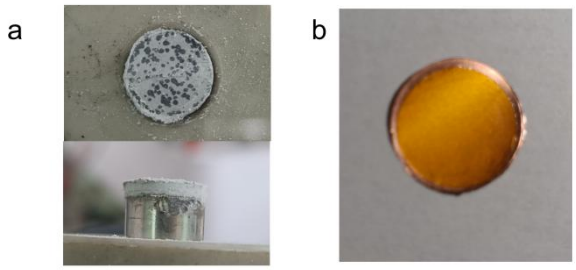

Figure S2. (a) Optical photographs of the surface of LPSC-PTFE near Cu side with a plating current density of 2 mA cm^{-2} and a cut-off capacity of 2 mAh cm^{-2}; (b) Optical photographs of Cu current collector with a piece of insulating tape.

As shown in Figure S2b, apply a PI tape with a diameter of 9 mm to the center of the copper foil, so that only the edges can achieve electron conduction.

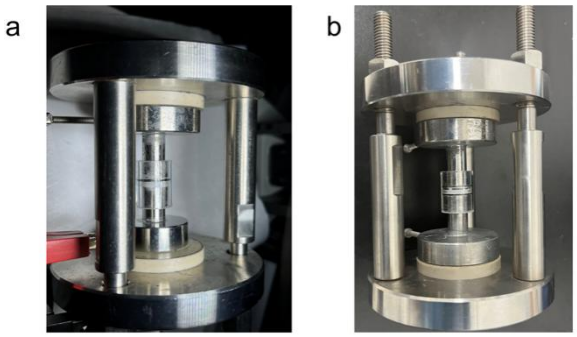

Figure S3. Optical photographs of the Li|LPSC|LPSC-PTFE|LPSC|Cu cell encapsulated in a quartz mold. (a) Before plating; (b) After plating.

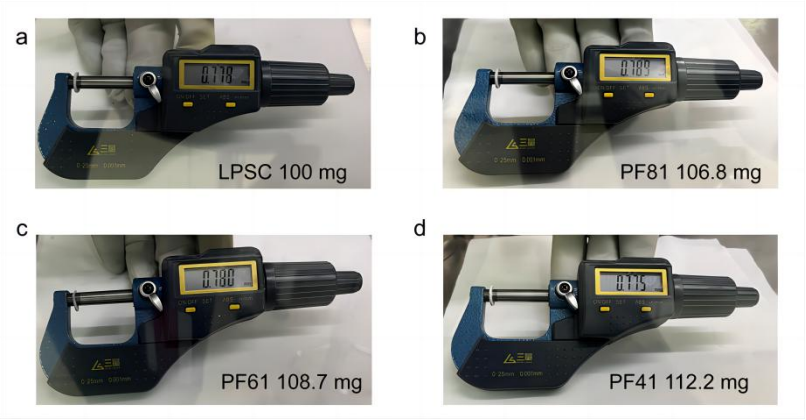

Figure S4. Thickness of (a) 100 mg LPSC, (b) 106.8 mg PF81, (c) 108.7 mg PF61and (d) 112.2 mg PF41.

Figure S5. Thickness of 110 mg LPSC (100 mg) -PTFE (10 mg) layer.

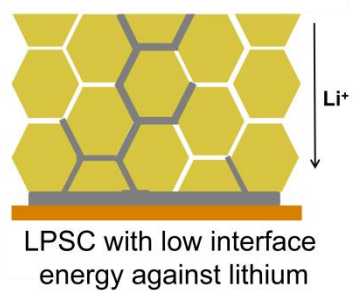

Figure S6. Schematic diagram of the dendrite growth mechanism, along the pre-existing chains of defects

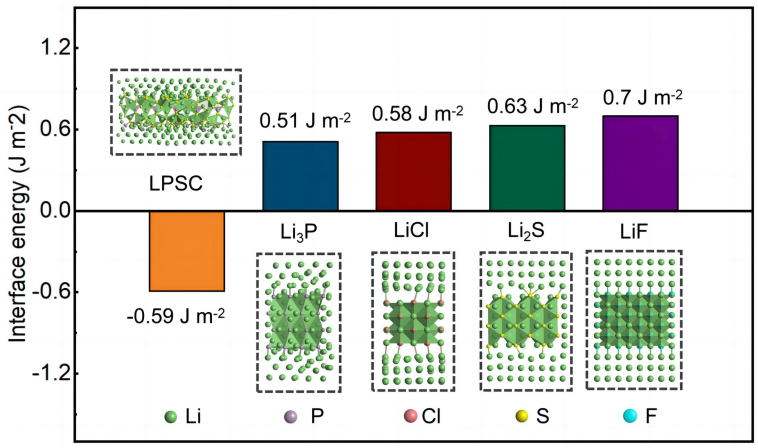

Figure S7. DFT calculated interface energies of LPSC, Li_3P, LiCl, Li_2S, LiF against lithium and relaxed Li/LPSC, Li/Li_3P, Li/LiCl, Li/Li_2S and Li/LiF interface (inset). Color code: green, Li atoms; purple, P atoms; pink, Cl atoms; yellow, S atoms; blue, F atoms.

As shown in Figure S7, density functional theory (DFT) calculation results show that the interface energy of LPSC against lithium metal is -0.59 J m^{-2}, and the negative interface energy means that LPSC will spontaneously react with lithium metal, and the decomposition products generated at the LPSC-Li interface are Li_2S, Li_3P and LiCl. Although the interface energy of Li_2S, Li_3P and LiCl against lithium metal in the decomposition layer is positive, the effect of these decomposition products on improving the dendrite blocking ability of LPSC is limited, and short circuit is still easy to occur in the LPSC electrolyte. Considering that the interface energy of LiF is higher than LPSC, Li_2S, Li_3P and LiCl, we designed a LPSC-LIF composite electrolyte which can withstand a high current density and realize a long cycle life.

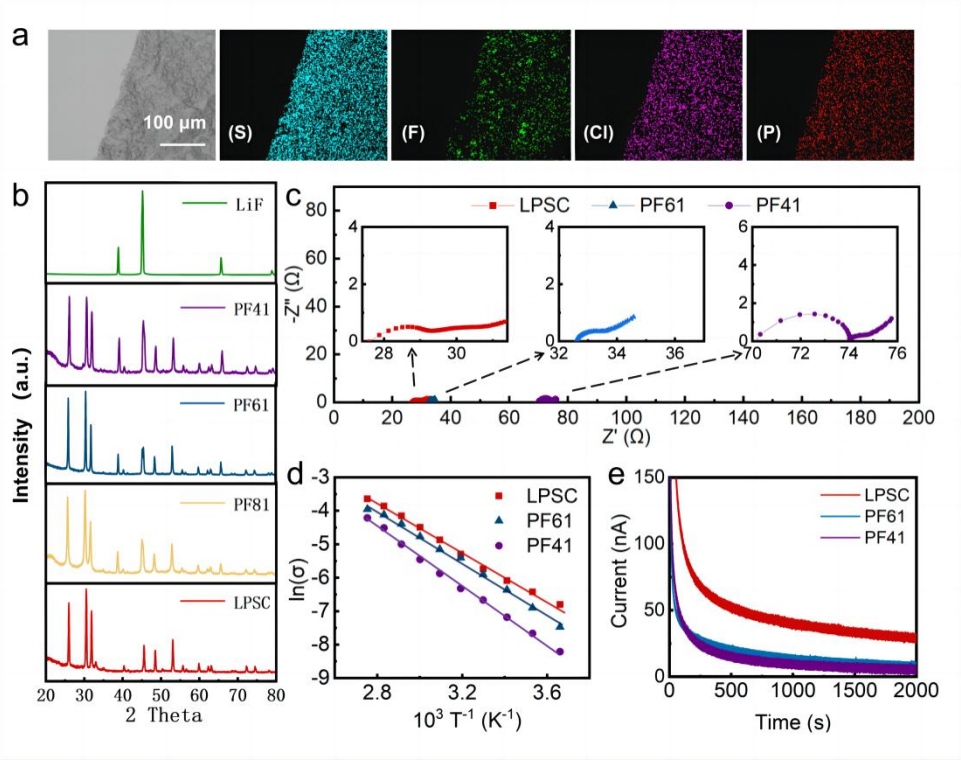

Figure S8. (a) SEM image and the corresponding S, F, Cl and P element mapping of PF61; (b) XRD patterns of LPSC, LiF and as-prepared LPSC-LiF electrolytes; (c) Nyquist plots of LPSC, PF61 and PF41 at 30 °C; (d) Arrhenius plots of the temperature-dependent ionic conductivities of LPSC, PF61 and PF41; (e) Current response of LPSC, PF61 and PF41 at a voltage of 0.5 V.

To investigate the effect of the amount of LiF incorporation on the properties of LPSC, a series of LPSC-LiF composite electrolytes were prepared and labeled as PF81, PF61 and PF41 according to the volume ratio of LPSC to LiF (see experimental section 1.1 for details). It is necessary to verify that the two materials can be mixed evenly by a simple ball milling, and the EDX analysis was employed. As shown in Figure S8a, S9 and S10, F is just as evenly distributed in the electrolyte as P, Cl, and S. Therefore, we can reasonably conclude that LiF is uniformly incorporated into LPSC. Secondly, in order to inhibit dendrite growth by the high interface energy against lithium of LiF, the existence form of LiF in the composite electrolytes must be identified, and XRD analysis was employed. As shown in Figure S8b, XRD patterns show that no matter how much LiF is added, the position of the characteristic peaks of LPSC and LiF does not change. And with the increase of LiF incorporation, the relative strength of LiF characteristic peaks in samples increased. This indicates that the crystal lattice of LPSC and LiF does not change during the simple ball milling process, and no chemical reaction occurs between them.

The ionic conductivities of LPSC-LiF electrolytes were evaluated by electrochemical impedance spectroscopy (EIS). Figure S8c, S8d and Figure S11 show the typical Nyquist

plots and the corresponding Arrhenius curves. Due to the strong electrostatic interaction between F ion and Li ion, the ionic conductivity of LiF is very low. It is inevitable that the incorporation of LiF will reduce the ionic conductivity of electrolyte. The ionic conductivity of pure LPSC is 4.0×10^{-3} S cm^{-1} at room temperature, which is similar to the values reported in the literatures.[7] The ionic conductivity of PF81 and PF61 at room temperature is 3.5×10^{-3} S cm^{-1} and 3.4×10^{-3} S cm^{-1}, respectively, which is slightly lower than that of pure LPSC, indicating that the addition of a small amount of LiF has little effect on the overall ionic conductivity of electrolytes. The ionic conductivity of PF41 is 1.4×10^{-3} S cm^{-1}, which is significantly lower than that of pure LPSC. In addition, the corresponding activation energy of PF81 (0.31 eV) and PF61 (0.33 eV) calculated by the Arrhenius equation are comparable to that of the pure LPSC (0.30 eV), indicating that the incorporation of a small amount of LiF will not affect the transfer kinetics of lithium ions. However, the activation energy of PF41 is 0.38 eV, much higher than that of pure LPSC, indicating that the performance of LPSC will be greatly reduced by the incorporation of a large amount of LiF. Electron conductivity is another important performance index of solid electrolyte, which can be measured by Stainless steel|SSEs|Stainless steel symmetrical cells. A voltage of 0.5 V was applied to these symmetrical cells, and the current profiles are shown in Figure S8e. Obviously, the electronic conductivity of LPSC-LiF electrolytes decreases with the increase of LiF incorporation due to the extremely low electron conductivity of LiF. The calculated conductivity of LPSC, PF81, PF61 and PF41 is 6.1×10^{-9} S cm^{-1}, 4.1×10^{-9} S cm^{-1}, 1.3×10^{-9} S cm^{-1} and 0.4×10^{-9} S cm^{-1}, respectively, which meets the requirement of all solid-state batteries.

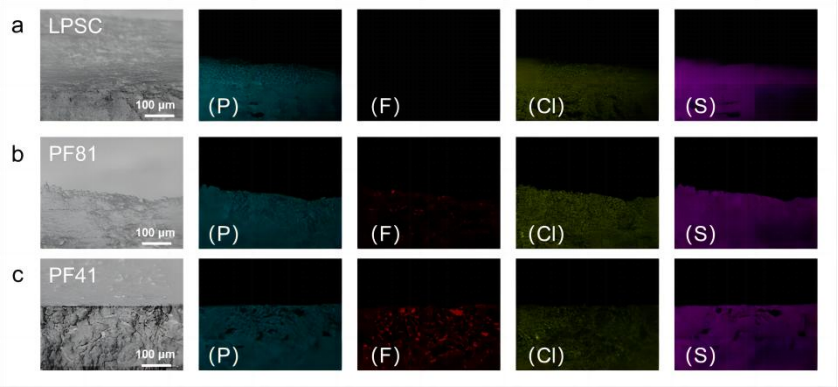

Figure S9. SEM image and the corresponding P, F, Cl and S element mapping of (a) LPSC, (b) PF81 and (c) PF41.

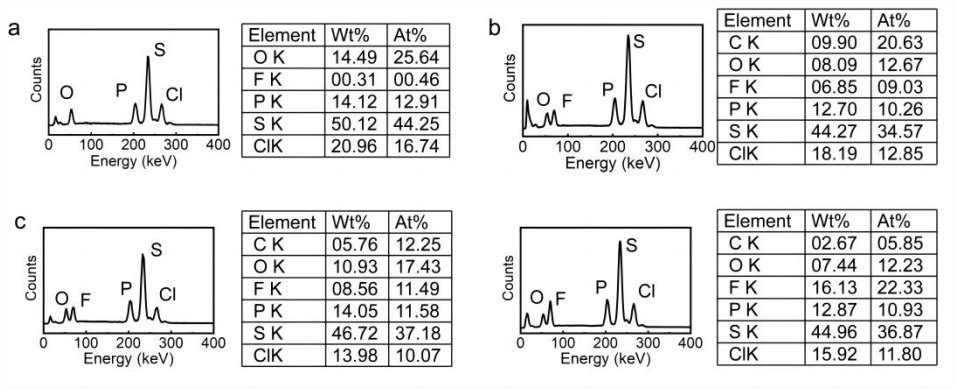

Element	Wt%	At%
O K	14.49	25.64
F K	00.31	00.46
P K	14.12	12.91
S K	50.12	44.25
ClK	20.96	16.74

Element	Wt%	At%
C K	09.90	20.63
O K	08.09	12.67
F K	06.85	09.03
P K	12.70	10.26
S K	44.27	34.57
ClK	18.19	12.85

Element	Wt%	At%
C K	05.76	12.25
O K	10.93	17.43
F K	08.56	11.49
P K	14.05	11.58
S K	46.72	37.18
ClK	13.98	10.07

Element	Wt%	At%
C K	02.67	05.85
O K	07.44	12.23
F K	16.13	22.33
P K	12.87	10.93
S K	44.96	36.87
ClK	15.92	11.80

Figure S10. EDS spectrum of (a) LPSC, (b) PF81, (c) PF61 and (d) PF41.

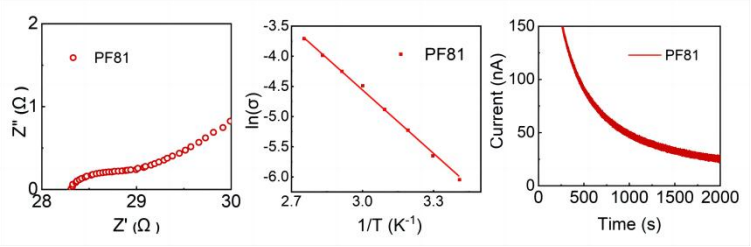

Figure S11. (a) EIS tests of Li|Li symmetric cell with PF81 at 30°C; (b) Arrhenius plots of the temperature-dependent ionic conductivities of PF81; (c) Current response of PF81 at a voltage of 0.5 V.

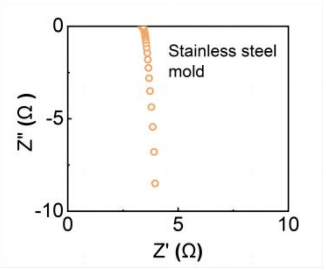

Figure S12. EIS tests of Stainless-steel mold.

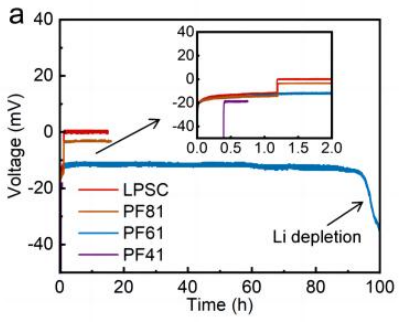

Figure S13. Voltage profiles of the Li|SSEs|Cu cells at a plating current density of 0.3 mA cm^{-2}, Color code: red, LPSC; brown, PF81; blue, PF61; purple, PF41.

Li|SSEs|Cu half cells were used to evaluate the ability of SSEs to suppress lithium dendrites. Figure S13 shows typical voltage profiles of lithium metal deposited on Cu

electrode with different electrolytes at 0.3 mA cm^{-2}.The illustration provides magnified views of the voltage profiles during the initial deposition of lithium metal. As shown by the red curve, the half-cell using pure LPSC could deposit lithium for about 1 h before a short circuit occurred, as indicated by the sudden step in the voltage. As shown by the brown curve, a half cell using PF81 could also deposit lithium for only about 1 h before short circuiting, indicating that a small amount of LiF doping cannot to improve the ability of SSEs to suppress dendrites. As shown by the blue curve, a half cell using PF61 could stably deposit lithium for 100 h without short circuit, and the increase in voltage at the end of the curve was caused by the depletion of the lithium source. Surprisingly, a half cell using PF41 not only had high deposition overpotential, but also rapidly experienced a short circuit after 0.5 h of lithium deposition, as shown by the purple curve. We speculate that this was caused by the poor ion conductivity of LiF. Adding a large amount of LiF will increase the effective current density through the LPSC, which will accelerate the short circuit of the cell. In addition, Li|PF61|Cu cell could still stably deposit lithium at a higher current density of 0.5 mA cm^{-2}, as shown in Figure S14.

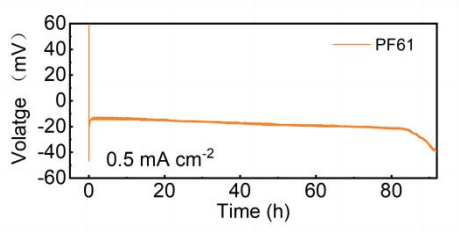

Figure S14. Voltage profiles of the Li|PF61|Cu cell at a plating current density of 0.5 mA cm^{-2}.

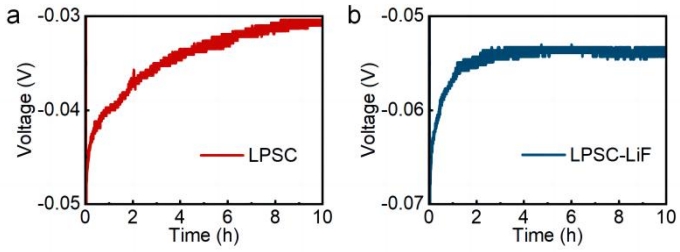

Figure S15. Voltage profiles of (a) the Li|LPSC|LPSC-PTFE|LPSC|Cu cell and (b) the Li|LPSC|LPSC-PTFE|LPSC-LiF|Cu cell at a plating current density of 0.3 mA cm^{-2}.

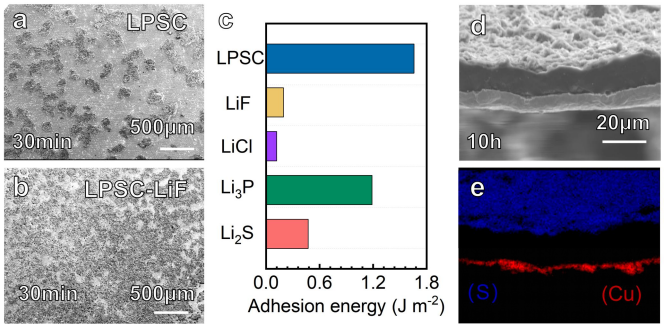

Figure S16. SEM image of Cu electrode peeled off from (a) the Li|LPSC|Cu half-cell and (b) the Li|LPSC-LiF|Cu half-cell with a current density of 0.3 mA cm^{-2} and a capacity of 0.15 mAh cm^{-2}. (c) DFT calculated adhesion energies of LPSC, Li_3P, LiCl, Li_2S, LiF against lithium. (d) SEM image of the Li deposit on Cu electrode and (e) the corresponding S and Cu element mapping.

The effect of LiF incorporation on the plating behavior of lithium was also investigated. Li|SSEs|Cu half cells were used to collect the Cu electrode plated with lithium. In order to avoid the short circuit of the Li|LPSC|Cu cell, the plating process is limited at a current density of 0.3 mA cm^{-2} and a capacity of 0.15 mAh cm^{-2}. Figure S16a shows the SEM image of Cu electrode peeled off from the Li|LPSC|Cu cell, the plated lithium was sparsely distributed on the surface of Cu foil as islands. Figure S17a shows an optical image of the side of the LPSC detached from the Cu electrode, a large amount of lithium sticked to the surface of LPSC, and even some of the lithium had entered the LPSC interior. In contrast, Figure S16b shows the SEM image of Cu electrode peeled off from the Li|LPSC-LiF|Cu half-cell, the plated lithium was uniformly and densely distributed on the surface of the Cu electrode. Figure S17b shows an optical image of the side of the LPSC-LiF detached from the Cu electrode, less lithium sticked to the surface of the LPSC-LiF, let alone entered the electrolyte interior. These phenomena can be well illustrated by the DFT calculation of the adhesion energy of electrolyte to lithium. As shown in Figure S16c, the adhesion energy of pure LPSC against lithium was much higher than that of LiF against lithium, so the deposited Li was more inclined to bond with pure LPSC. Due to the incorporation of LiF, the adhesion energy of LPSC-LiF against lithium was significantly decreased, and the deposited Li was more inclined to bond with Cu electrode. Given that the LPSC-LiF exhibits excellent lithium dendrite inhibition in electrochemical tests, the cross-section of Cu electrode detached from Li|LPSC-LiF|Cu half-cell with a high plating capacity of 3 mAh cm^{-2} was further observed. As shown in Figure S16d and S16e, lithium could be uniformly plated, and the elemental analysis clearly shows the distribution of Cu, plated lithium and electrolyte adhering to lithium.

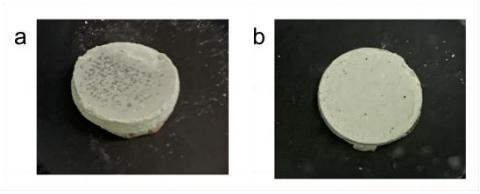

Figure S17. Optical photographs of the surface of (a)LPSC and (b) LPSC-LiF near Cu electrode, after lithium plating for 0.5 h at a current density of 0.3 mA cm^{-2}.

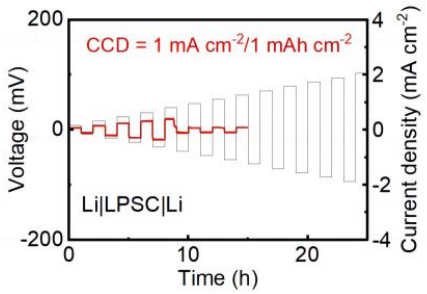

Figure S18. Critical current density of the Li|LPSC|Li symmetric cell at room temperature.

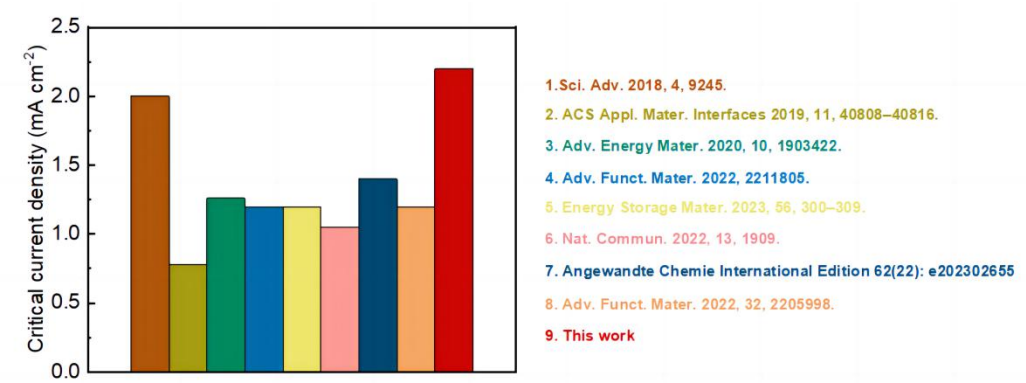

Figure S19. Comparison of critical current densities of the Li|Li cells in this work with those in the literature.

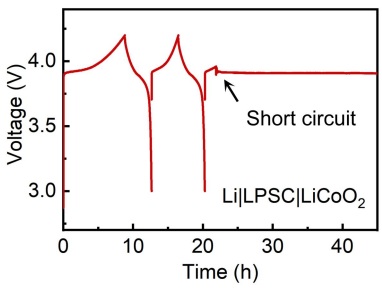

Figure S20. Charge–discharge profiles of the Li|LPSC|$LiCoO_2$ cell at 0.1C.

As shown in Figure S20, the Li|LPSC|$LiCoO_2$ cell delivered an initial discharge capacity of 76.6 mAh g^{-1} and a Coulombic efficiency of 86.9% at 0.1 C. The poor electrochemical performances should be ascribed to the side reaction of the LPSC at the electrode-electrolyte interface, which leads to large polarization and poor reversibility. And the Li|LPSC|$LiCoO_2$ cell quickly short-circuited on the third electrochemical cycle due to dendrites passing through the electrolyte.

References

1 Kresse, G.; Furthmüller, J. Efficient Iterative Schemes for Ab Initio Total-Energy Calculations Using a Plane-Wave Basis Set. Phys. Rev. B: Condens. Matter Mater. Phys. 1996, 54, 11169−11186.

2 G. Kresse and D. Joubert, Physical Review B, 59, 1758 (1999)

3 Monkhorst, H. J., and J. D. Pack. "Special Points for Brillouin-zone Integrations, Phys. Rev. B, 13, p. 5188." (1976).

4 Jain, Anubhav, et al. "Commentary: The Materials Project: A materials genome approach

5 Lepley, N. D., and N. A. W. Holzwarth. "Modeling interfaces between solids: application to Li battery materials." Physical Review B 92.21 (2015): 214201.

6 Zhang, Z., et al., Flexible Sulfide Electrolyte Thin Membrane with Ultrahigh Ionic Conductivity for All-Solid-State Lithium Batteries. Nano Letters, 2021. 21(12): p. 5233-5239.

7 Unprecedented Self-Healing Effect of Li6PS5Cl-Based All-Solid-State Lithium Battery. Small, 2021. 17(37): p. 2101326.